Polarisation singularities on plasmonic nanowires

Author:
Nicolaas van der Voort

Supervisors:
Prof. Kobus Kuipers
MSc. Anouk de Hoogh

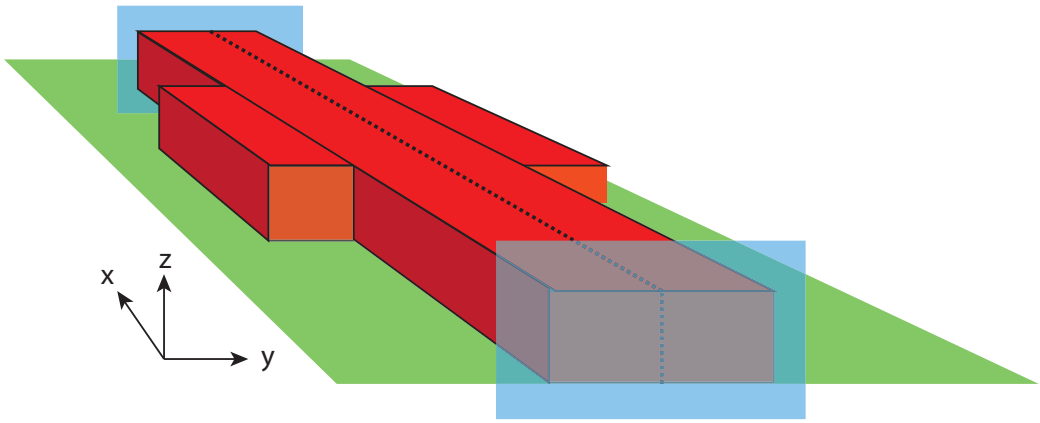

Thesis to obtain the Bachelors degree
in Physics and Astronomy at the University of Utrecht

Performed at AMOLF, FOM institute for nanoscience
Nano Optics group, center for Nanophotonics

June 16, 2013

Abstract

Placing quantum dots at polarisation singularities is expected to allow for direct control over the directionality of the emitted light. Possibly creating a photon driven quantum bit. Here, we investigate the occurrence of polarisation singularities on plasmonic nanowires with periodic extrusions. We build a 3D model based on a finite element method in order to calculate the electric fields using Floquet periodicity and the theory of surface plasmons, propagating along the metal-dielectric interface.
To validate our model we first show qualitative agreement between results obtained with the 3D model and earlier 2D models of a straight wire. Secondly we develop a piece of mathematics that allows for determining polarisation singularities independent of a reference frame and we show that polarisation singularities exist on plasmonic nanowire with periodic extrusions at the surface of the metal.

Contents

1 Introduction **1**
- 1.1 SPP dispersion relation . . . 2
- 1.2 Sommerfeld and Bloch modes . . . 3
- 1.3 Outline . . . 4

2 3D modelling of plasmonic nanowires **5**
- 2.1 Introduction . . . 5
- 2.2 Methods . . . 5
  - 2.2.1 Floquet periodicity and Bloch modes . . . 5
  - 2.2.2 Finite element method . . . 8
  - 2.2.3 Perfect Magnetic Conductors . . . 9
  - 2.2.4 Eigenfrequency analysis . . . 9
- 2.3 SPP's on straight nanowires . . . 9
  - 2.3.1 Damping and Dispersion relations for $\vec{k}$ control variable 9
  - 2.3.2 Mode profile of guided SPP's . . . 11
  - 2.3.3 Dispersion curve around telecom frequencies . . . 11
- 2.4 Conclusions & discussion . . . 12

3 Singularities on periodic nanowires **14**
- 3.1 introduction . . . 14
- 3.2 Polarisation properties of electric fields . . . 14
- 3.3 Determining polarization singularities . . . 17
- 3.4 Field convergence behaviour for different mesh . . . 18
  - 3.4.1 Structural geometry . . . 18
  - 3.4.2 Mesh convergence . . . 19
- 3.5 Mode profiles . . . 20
- 3.6 Singularities at p-lines . . . 21
- 3.7 Conclusions and outlook . . . 23

Acknowledgements **27**

Chapter 1

Introduction

In 1965 Gordon Moore introduced his famous law stating that the amount of resistors on an integrated circuit will double every two years. Moore's law holds until the current date, however in recent years physicists are struggling to keep up because of the constraints posed by fundamental physical constants. Now, a new innovation is looming on the horizon. Recent developments in nanotechnology and nanostructuring enable us to create increasingly smaller and complex structures. Which in turn generates greater control of sub-wavelength behaviour and fine-structure of light, this field of research is now referred to as quantum optics. Controlling the emission of quantum emitters by coupling them to optical singularities on nanowires can achieve great spacial resolution, since the resolution of a singularity is by definition zero. This may pose a new step in the miniaturisation of computer components.
In this thesis we will investigate the occurrence of so-called C-points on plasmonic nanowires. In these C-points the light is perfectly circular polarized, which allows for a direct access to spin resolved optical excitation to quantum dots. In principle, this allows control over the emission of single quantum emitters by placing them at polarisation singularities. Imagine a spin-dependent transition of a quantum emitter. If the quantum emitter is placed at an optical singularity, the handedness of the transition determines the propagation direction of the light. If an emitted photon moves to one end of the nanowire, the photon will interact with the singularity as if it is right-handed, while if it moves to the other end, it will interact as if it is left-handed polarisation, or vice versa depending on the handedness of the singularity. Thus creating a great control over the directionality of the propagation. This allows for effectively determining the transition state and creating a qubit.
Previously it has been shown that these singularities exist at the nanoscale.[1]

They appear in abundance on photonic crystal waveguides, where every unit cell contains two C-points, separated by a space of 150nm. However, the appearance and behaviour of optical singularities on plasmonic nanowires is still unexplored. Breaking the symmetry in the length direction of the nanowires gives rise to more complicated mode profiles, consisting of multiple Fourier components, which may allow for the appearance of polarisation singularities away from the surface of the nanowire.

1.1 SPP dispersion relation

When photons couple to a metal / dielectric interface, for example by using a periodic hole array, the electric field of the photons can influence the charge carriers at the surface of the metal, creating a surface charge density wave at the interface. This quasi-particle is called a Surface Plasmon Polariton, henceforth referred to as a SPP. In order to obtain a better understanding of the behaviour of SPP's, we will shortly discuss it's physical properties. The surface charge density wave, propagating at the interface, has a $\vec{k}$ satisfying

$$nk_0 = \sqrt{k_x^2 + k_y^2 + k_z^2} \tag{1.1}$$

wherek_0 is the norm of the k-vector in vacuum, n is the refractive index of the material in which the wave propagates and k_i the component of the k-vector in direction i. Now consider a slab of metal, lying on a dielectric substrate. We consider a wave propagating at the interface between these materials. We choose the x- axes along the propagation direction of the wave and the z-axes perpendicular to the interface such that k_y is 0. A special situation occurs when one of the components is larger than k_0. Mathematically this is allowed for if the other components become imaginary. E.g. $k_x > k_0$, k_z is imaginary. When these values are entered in the wave equation 1.2 the y and z components become exponentially decaying function and the SPP wave is confined in the y and z direction. The larger the k_x component the more confined the wave becomes in the y- and z-direction.

$$\Psi(\vec{x}, t) = e^{i\vec{k}\vec{x} - \omega t} \tag{1.2}$$

With Ψ the wave function, $\vec{k}$ the k-vector consisting of k_x, k_y and k_z and ω the angular frequency. In case of a slab of metal on a dielectric surface, the wavevector $\vec{k}_x$ of the SPP on the interface between the metal and the dielectric, is related to the incident frequency ω according to the dispersion relation [2]

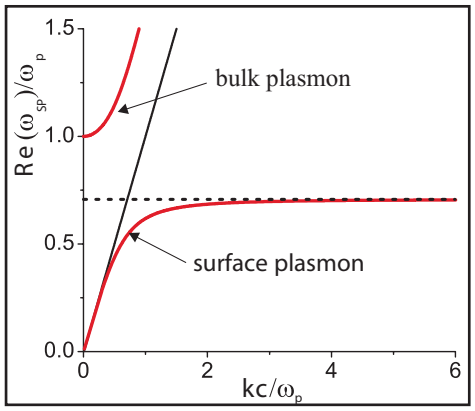

Figure 1.1: Dispersion relation of a SPP at the interface of a Drude metal with Air.

$$k_x = k_0 \sqrt{\frac{\epsilon_d \epsilon_m}{\epsilon_d + \epsilon_m}} \tag{1.3}$$

where ϵ_d is the dielectric constant of the dielectric and ϵ_m the dielectric constant of the metal. The dielectric constant of the metal is in turn dependent on the frequency of the incident light and can be described with the Drude model for a free electron gas [3].

$$\epsilon_{m,Drude}(\omega) = 1 - \frac{\omega_p^2}{\omega^2 + i\Gamma\omega} \tag{1.4}$$

Where ω_p is the plasma frequency for the metal and Γ is a damping rate depending on electron-electron and electron-phonon collisions. Combining these equations renders the dispersion relation, discussed further in section 2.3.1. For frequencies below the surface plasmon resonance frequency $\omega_{sp} = \omega_p/(1 + \epsilon_d)$, e.g. $\epsilon_m < \epsilon_d$, the SPP curve lies to the right of the light line and has a $k_x < k_0$. Accordingly, k_z is imaginary and there is confinement and guidance of the propagating wave. For $\omega > \omega_p$ the dispersion curve lies to the left of the light line, as a result $k_x < k_0$ and k_z becomes real through equation 1.1. Now the wave will travel from the dielectric-metal interface and it is no longer confined, resulting in radiation. This branch is therefore not of particular interest for guided SPP's on nanowires.

1.2 Sommerfeld and Bloch modes

Previous research has already investigated the mode profiles on straight nanowires [4, fig 2]. These so-called Sommerfeld-modes consist of one harmonic in the propagating direction and can have different shapes in the area

perpendicular to the propagating direction. When the cross-section is very small, e.g. for small waveguide widths, there is only enough room for the lowest order mode to exist, only half a wavelength fits into the cross section of the wire, the circumference of the cross section can be compared to the length of the box in the well known particle-in-a-box problem. When the box gets larger, e.g. the width of the waveguide increases, enough room is created for higher order modes to fit in. As a result, one wavelength or higher modes can exist in the box. The widths of the wire discussed in this thesis are sufficiently small for only the ground mode, associated with m = 0, to exist. For further reference on this area see [5]
When an incoming wave interacts with a periodic lattice, a Bloch modes arises. Bloch modes consist of a periodic part, multiplied by an enveloping wave. This periodic part can be expressed as a Fourier series of individual waves. In this sense it consists of many different wave, who all share the same angular frequency and propagation speed. This will be discussed further in Chapter 2.

1.3 Outline

Here, we have shortly discussed the dispersion relation and mode properties of surface plasmon polaritons on plasmonic nanowires. In the next chapter we introduce a 3D model to be able to simulate a model with broken symmetry in the propagating direction by creating a wire with periodic extrusions. There we will first compare results of the new 3D model and previous well-tested 2D models in case of a straight wire in order to show the validity in chapter 2. In chapter 3 we discuss the mathematics needed to analyse polarisation singularities independent of their reference frame and we use the new 3D model of the nanowire with extrusions to investigate polarisation singularities. We finish considering the conclusions and implications of this study and look towards the future for future research and applications.

Chapter 2

3D modelling of plasmonic nanowires

2.1 Introduction

The behaviour and dispersion relation of guided SPP's on nanowires is studied extensively and reported in literature thoroughly [6]. Due to the geometric symmetry in the propagating direction of the nanowire, calculations on these wires can be done in 2D. Therefore in previous studies 2D simulations have been used frequently. However for the purpose of investigating nanowires with extrusions on the side, as can be seen in figure 3.2, the geometric symmetry is broken and modelling in 3D is necessary. In this chapter we will simulate a 3D straight wire, as seen in figure 2.1, as a test case and compare the results with previously obtained results from 2D models.

2.2 Methods

These simulations are performed in the environment of the Comsol software packet. The installed version is 4.2 with the added Rf-module, run on an 8-core calculation server with 128 Gigabytes of RAM.

2.2.1 Floquet periodicity and Bloch modes

In 2D modelling a cross cut in the yz direction from figure 2.1 is taken and due to symmetry in the propagating direction, the simulation is done for an infinitely long wire. In 3D modelling no such symmetry can be used, however the aim is still to model for an infinitely long wire, this is necessary to prevent unwanted boundary effects. It is also crucial to limit the size of the model

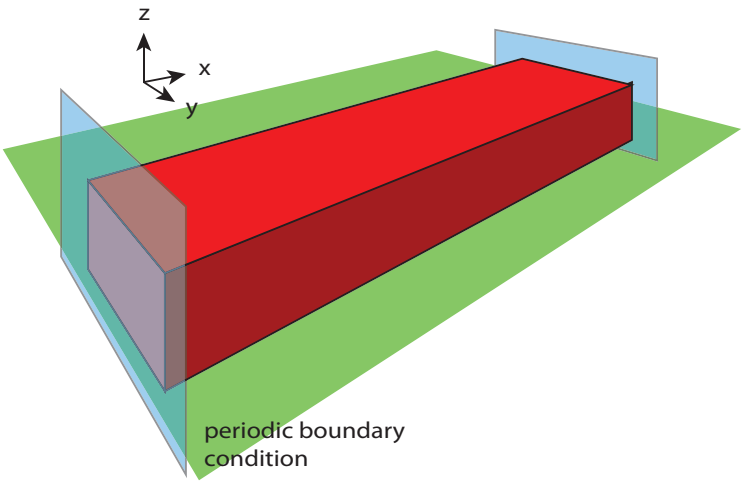

Figure 2.1: schematic view on the 3D model of a straight wire with periodic boundary conditions. The green plane shows the glass substrate

due to the very fast increase in calculation effort in 3D modelling. The main issue is the limitation in RAM available on the server. This can be solved by using periodic boundary conditions. In case of a periodic structure, each period is concatenated with the next period, indicated with the blue planes. The Electric fields associated with a periodic structure can be found using Floquet Theory. For a comprehensive view on Floquet periodicity, please refer to [7]. Floquet theory is based on the assumption that the shape of the mode profile is the same for each period. It does allow for an amplitude and phase shift. I.e. the periodicity of the structure forces the interacting field to have the same periodicity. The shift in a complex amplitude u in a one dimensional case is given by $u(x + L) = Cu(x)$, where L is the length of one periodicity. For multiple periods this becomes $u(x + nL) = C^n u(x)$. Please note that time-dependency is disregarded. The factor C is a complex number, which allows for both an amplitude as well as a phase shift. In case of a bounded wave there is an extra condition $|C| < 1$ and can be written in general as e^{ikL}. In this equation k is some complex number which allows for both an amplitude change as well as a phase shift.
If u(x) consists of exactly a periodic part and a complex exponential part, this allows exactly for the aforementioned property. E.g. $u(x) = e^{ikx}P(x)$. Since P(x) is a periodic function, it can be described as a Fourier series. As a result the total function u(x) can also be written as a Fourier series.

$$P(x) = \sum_{n=-\infty}^{\infty} c_n e^{\frac{i2\pi n}{L}x} \tag{2.1}$$

$$u(x) = \sum_{n=-\infty}^{\infty} c_n e^{(\frac{i2\pi n}{L}+k)x} \tag{2.2}$$

Formulated this way, u(x) can be interpreted as a series of waves which all have the same phase and amplitude shift compared to the next period. The mode profile remains the same no matter which period we look at. We have now satisfied our original assumption and created a Bloch wave. For a given phase shift k, a unique solution of c_n factors exist, which describe the profile of the mode. The amplitude change is also determined for a given phase-shift. Since the phase-shift generates a mode profile, the electric field interacts with the geometrical and material system properties, the decrease in amplitude or damping coefficient is then determined by this interaction, this property is determined also by the phase shift.

The schematic dispersion relation of such a Bloch wave is also periodic (see fig 2.2), since the function u(x) is periodic in $2\pi/L$. If the length of one period $2\pi/L$ is added to a given complex phase shift k, the resulting sum of harmonics remains the same and the modes are equal.

$$\sum_{n=-\infty}^{\infty} c_n e^{(\frac{i2\pi n}{L}+k+\frac{2\pi}{L})x} = \sum_{n=-\infty}^{\infty} c_n e^{(\frac{i2\pi(n+1)}{L}+k)x} \tag{2.3}$$

Same color arrows illustrate that different component separated by $2\pi/L$ all contribute to same Bloch mode. From this figure, all k-vectors that contribute to one Bloch mode have the same group velocity (same slope) and the same energy.

Floquet theory was developed to be applied to periodic structures, however it is not very applicable to the situation of an infinitely long wire since this structure has no periodicity. The theory imposes boundary conditions which are not inherently satisfied by the model. Used on a straight wire the mode is allowed to consists of an infinite number of k-vectors, according to equation 2.2. However in the case of a straight wire the mode consists of only one component and as a result only one of the allowed k-vectors will be dominant. The set of k-vectors however, depend on the length of the periodicity, since there is symmetry in for any length we choose, it can be chosen at will. This problem can be circumvented by choosing a k-vector such that it corresponds to a mode we want to find and by choosing the periodicity sufficiently small, such that only one k-vector lies in the regime of possible found modes.

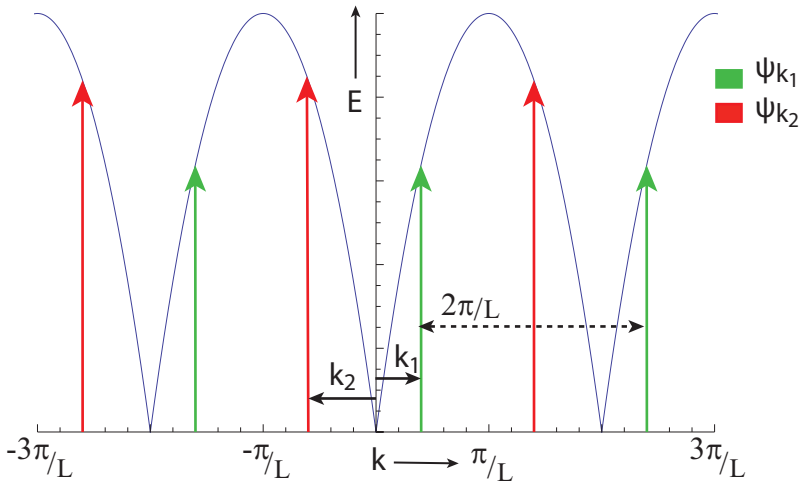

Figure 2.2: Schematic photon dispersion relation on a periodic lattice, with lattice constant L. Three periods of the first band have been drawn. Same color arrows contribute to the same Mode.

2.2.2 Finite element method

The solutions found in this simulation are obtained with a finite element method (FEM). In this paragraph the basic properties of the simulation method are describes in order to create some insight into the underlying mechanisms.
FEM is needed when a solution to a boundary problem can no longer be found analytically. It divides the geometry into smaller subdomains, called finite elements. Together these elements form a mesh. Each subdomain is related to other subdomains in this case by Maxwell's equations. FEM encompasses all the methods to connect these small elements and find the best approximation.
Mathematically the interaction between the finite elements is given by a Hamiltonian matrix, in which the n^{th} row denotes how the n^{th} element is affected by all other elements. Then a trial solution in the form of a vector is needed and it becomes an eigenvalue problem. After the hamiltonian is applied to the trial solutions, a different solutions is generated. The difference between these two vectors becomes an error function. When the error function becomes zero, an eigenmode has been found. Several methods exist to minimize this error function [8].

Mesh

As mentioned, it is very important to increase the efficiency of the calculation. One of the key possibilities to accomplish this is by optimizing the design of the mesh. This is done by creating a fine mesh in areas where you would expect fluctuations, In this case in areas with a high field amplitude near edges and boundaries of the nanowire. A more course mesh can be created in areas of less interest. If a mesh is too course, local field effects can be missed. It is necessary to be careful here; if one chooses poorly it is possible to miss local field effects.

2.2.3 Perfect Magnetic Conductors

In the geometry of a rectangular wire there is a symmetry plane in the xz-plane as seen in figure 2.1. We will use this symmetry to cut the size of the model in half and decrease RAM usage. This symmetry plane is implemented with the help of Perfect Magnetic Conductors (PMC's) [9]. PMC's work in a similar way as perfect electric conductors. A PMC allows no magnetic field in the material and as such there are no electric currents in the material. This forces the tangential component of the magnetic field to be zero, which is the property of the symmetry plane that is created.

2.2.4 Eigenfrequency analysis

Floquet's theorem generates a solution depending on the phase change between two periods denoted with $\vec{k}$. For simulation purposes it is therefore required to have $\vec{k}$ as input. In order to meet this requirement we have used an eigenfrequency analysis method. This method calculates the eigenmode profile using a FEM given a Floquet k-vector and derives the resulting eigenfrequency. The mode consists of a Fourier series as in 2.2, in which k is given in the three-dimensional case by $\vec{k}$. Since the calculated mode is an *eigen*mode, no external excitation source is needed and the amplitude of the mode can be normalised at will.

2.3 SPP's on straight nanowires

2.3.1 Damping and Dispersion relations for $\vec{k}$ control variable

To create a realistic model it is necessary to account for damping. Considering the general wave equation 1.2, there are two places where damping can

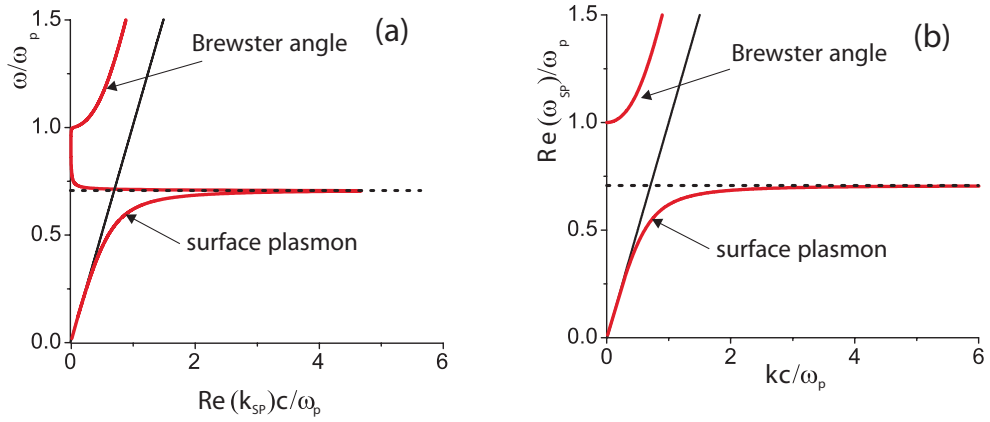

Figure 2.3: Dispersion relation for ω (a) and k (b) as control variables. The black solid line indicates the light line, on the left side of the line the light is radiative and on the right side it is evanescent and bound to the surface. The dashed line indicates surface plasmon resonance. *From: Phys. Rev. B79 195414, Surface Plasmon Fourier optics, Archembault et al. [10]*

be inserted. In a complex part of ω and a complex part of $\vec{k}$. Mathematically both render a negative exponential that provides for damping. However, they represent different physical situations.
In case of a complex k-vector the damping occurs as a function of distance, it can be compared to the situation where a constant source produces light, as we move away from the source, more of it is absorbed. A complex ω renders damping in time and can be compared to the decrease in amplitude when a guitar string is toggled. Due to the Floquet periodicity condition a k-vector is needed as input. Since the damping can not be determined beforehand, since it is a result of the interaction between the electric field and the geometry, the input k-vector is chosen as real, resulting in a complex ω. This is an artefact of the simulation requirement and not the result of a physical situation.

As shown by Archambault et al. [10], the dispersion relation of guided SPP's on flat metal-dielectric interface is different depending on whether $\vec{k}$ or ω is chosen as control variable. See figure 2.3. As mentioned, when ω is chosen as control variable, the resulting k-vector is complex and vice versa. The main difference in the dispersion relation is visible at $\omega_{sp}/\sqrt{2}$, chosen for a metal/air interface, where ϵ_d is 1. The difference in dispersion relation is caused by over-damping at $\omega_{sp}/\sqrt{2}$. If ω is the control variable, the damping

is so great that the wave is extinguished before it can cycle trough one period, therefore no k-vector can effectively be determined and the dispersion curve bends back.
In general these two curves differ when damping is present and it can be expected that a different solution is found when $\vec{k}$ is used as control variable, instead of ω.

2.3.2 Mode profile of guided SPP's

Due to symmetry and anti-symmetry conditions of the transfer functions $T_{\vec{x}\vec{u}}$, there must be symmetry in the x- and z- components of the electric field of the eigenmode and antisymmetry in the y-component, as viewed from the xy scanning plane [4]. $T_{\vec{x}\vec{u}}$ denotes the transfer functions from the electric field with dimensions $\vec{x} = \{x, y, z\}$ into a near-field scanning tip with polarisation directions $\vec{u} = \{u, v\}$. It is expressed as a matrix here. This property holds for all eigenmodes on a straight plasmonic wire.
As can be seen from figure 2.4, we show symmetry in the E_x and E_z and anti-symmetry in E_y. In order to compare with existing results obtained with a near-field setup, it is necessary to compare the area outside of the nanowire in (c) and the area inside of the nanowire in (d) with the scanning probe image. Please note that there is a significant longitudinal x-component, that also largely exists inside the metal wire. We see a good correspondence between the obtained mode profile here and in earlier results.

2.3.3 Dispersion curve around telecom frequencies

As a quantitative test for the model a dispersion curve is measured around telecom frequencies. From the calculation 2 branches are found, shown in figure 2.5. Both curves have been fitted with a linear fit to calculate their slopes. The actual dispersion relation is probably not linear, however, since we investigate only a small area of the dispersion curve, this approximation can be made.

Comparing figure 2.5 with 2.3 we see that for branch 1, denoted with ω_1 the dispersion curve has a positive slope. For branch 2 the dispersion relation has a negative slope and a refractive index which decreases as a function of the ω. This deviates from previously obtained results.

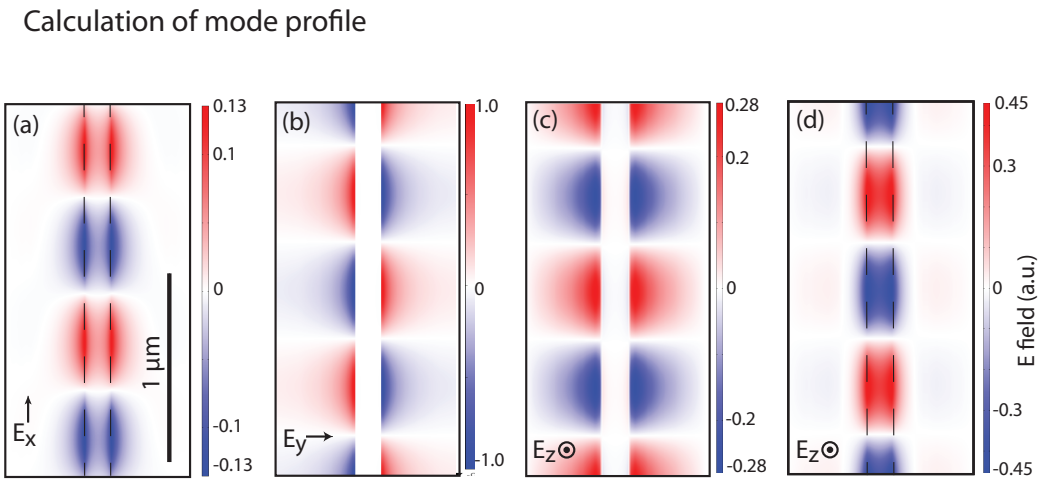

Figure 2.4: Mode profile of a guided mode on a plasmonic nanowire. (a,b,c) are taken 20 nm above the substrate, (d) is taken 20 nm above the sample, 120nm above substrate. Dashed lines indicate the edge of the nanowire. The amplitude of the electric field is normalised to the highest amplitude encountered in all the plots. The number at the top of the color scale indicate the maximum value of that plot.

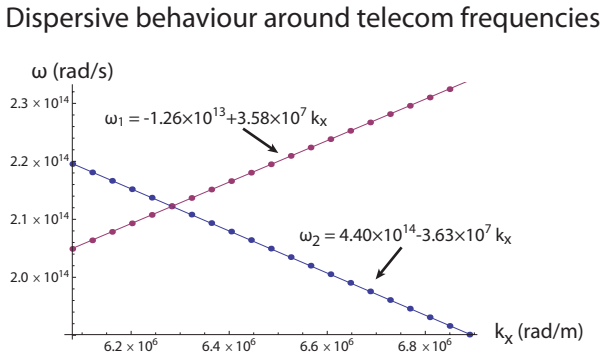

Figure 2.5: Part of the dispersion curve for 80nm wide and 100 high plasmonic nanowires for frequencies around telecom frequency (1550nm) as a function of k_x. Two branches are found. The numbers in the fit show the fitted linear function.

2.4 Conclusions & discussion

We have shown that it is possible to simulate 3D nanowires using Floquet Theory. We show that the 3D model exhibits a number of the same properties as the 2D model and theory on plasmonic nanowires predicts. We see

good correspondence in the shape of the mode profile and we find symmetry in the x- and z- direction and antisymmetry in the y-direction of the electric field. We have shown that it is possible to create a dispersion relation using Floquet theory and 3D modelling.

In order to fully ascertain the validity of this 3D model, it is necessary to show quantitative agreement between this 3D model and earlier 2D models. Now we have shown that there exists qualitative agreement with earlier models. Not everything in figure 2.5 can be explained yet. Branch 1 can be part of a dispersion curve, however this is not completely apparent yet and further measurements are needed. Difficulties arise when the k-vector dependent Floquet periodicity is introduced. As mentioned in section 2.2.1, the k-value used here as a control variable is actually a derived variable, i.e. it changes as a function of the wire width and height, where the frequency is independent of all these boundary conditions. The difference between ω or $\vec{k}$ introduces further problems. On top of that Floquet periodicity allows for an infinite series of k-vectors and forces a periodic dispersion upon the system, the found eigenmode consists of only one of these vectors, therefore it is possible that this vector differs from the original input $\vec{k}$ by a factor of $(2\pi n)/L$ for any integer n, therewith making it hard to determine the dominant k-vector in the Fourier spectrum. Further investigation is needed to account for these and possibly other effects and reach good quantitative agreement.

Chapter 3

Singularities on periodic nanowires

3.1 introduction

Many new techniques in the field of nanofabrication and nanotechnology have given the possibility to create increasingly complex structures at the nanoscale. These previously unattainable possibilities allow for an increasing control over the fine structure of light. Periodic constraints disturb the single harmonic propagation found in straight nanowires and give rise to more complicated mode profiles, consisting of multiple harmonics. These complicated structures and mode profiles may allow for polarization singularities to exist. However, it is practically impossible to predict where and with which structures they will occur, therefore simulation is needed.

3.2 Polarisation properties of electric fields

Every point of an electric light field in general has a polarisation, i.e. the precession of the electric field vector in time. Each complex vector component has an amplitude and a phase, which determines how that component will change in time. In general combining these vector components results in an elliptic polarisation, since we assume there are now special conditions for the amplitude and the phase. In a special case linear- and circular polarisation can exist. Linear polarisation can be considered consisting of two circularly polarised waves with opposite handedness.
For simulation purposes it is not necessary to modulate fields in time. Rather, a snapshot is taken of the field, in which every point is expressed as three complex numbers for each direction, from the ω dependance time evolution

follows. The norm of the complex number denotes the maximum amplitude of that point and the phase denotes in which part of the precession it is currently in. E.g. $1 + i$ denotes the component which will behave as $\sqrt{2}\cos(\omega t + \pi/2)$, with ω being determined by the entire system. It is the same for all points. Light in vacuum only has components perpendicular to the propagating direction, then it is sufficient to calculate only two components. However, breaking the symmetry in the propagating direction also allows for an electric field component in the propagating direction, so that it is necessary to account for all three dimensions. The rotation ellipse is still defined in some plane, however this plane is now no longer fixed and varies as a function of position. The polarisation properties of the electric field van be quantized using the following derivation [11, p. 34-36].

$$\vec{E}(\mathbf{r}) = \vec{p}(\mathbf{r}) + i\vec{q}(\mathbf{r}) \tag{3.1}$$

With $\mathbf{r}$ denoting the position dependency. The electric field in each point can be described as a real vector $\vec{p}$ and an imaginary vector $\vec{q}$. Now neglecting the $\mathbf{r}$ dependency, this can be expressed as

$$\vec{p} + i\vec{q} = (\vec{a} + i\vec{b})e^{i\alpha} \tag{3.2}$$

With α being any scalar. Now we can express $\vec{a}$ and $\vec{b}$ in terms of $\vec{p}$ and $\vec{q}$.

$$\begin{aligned} \vec{a} &= \vec{p}\cos(\alpha) + \vec{q}\sin(\alpha) \\ \vec{b} &= -\vec{p}\sin(\alpha) + \vec{q}\cos(\alpha) \end{aligned} \tag{3.3}$$

If α can have any value, it can be chosen such that $\vec{a}$ and $\vec{b}$ are orthogonal and that $|\vec{a}| \geq |\vec{b}|$.

$$(\vec{p}\cos(\alpha) + \vec{q}\sin(\alpha)) \cdot (-\vec{p}\sin(\alpha) + \vec{q}\cos(\alpha)) = 0 \tag{3.4}$$

$$\tan(2\alpha) = \frac{2\vec{p} \cdot \vec{q}}{\vec{p}^2 - \vec{q}^2} \tag{3.5}$$

The real part is taken from 3.2 and the time dependency is taken into account.

$$\Re[(\vec{a} + i\vec{b})e^{-i(\omega t - \alpha)}] = \vec{a}\cos(\omega t - \alpha) + \vec{b}\sin(\omega t - \alpha) \tag{3.6}$$

Remember that α is chosen such that $\vec{a}$ and $\vec{b}$ are orthogonal, and so 3.6 describes an ellipse with long axes $\vec{a}$ and short axes $\vec{b}$. We can now determine

the ellipticity, which is defined as the short axes divided by the long axes. Using equations 3.3 and 3.4 we obtain the following relations.

$$\begin{aligned} a^2 &= \frac{1}{2}[p^2 + q^2 + \sqrt{(p^2 - q^2)^2 + (2\vec{p} \cdot \vec{q})^2}] \\ b^2 &= \frac{1}{2}[p^2 + q^2 - \sqrt{(p^2 - q^2)^2 + (2\vec{p} \cdot \vec{q})^2}] \end{aligned} \tag{3.7}$$

Now the ellipticity ϵ, which is the ratio between the short axes and the long axes, is given by

$$\epsilon = \frac{p^2 + q^2 + \sqrt{(p^2 - q^2)^2 + (2\vec{p} \cdot \vec{q})^2}}{p^2 + q^2 - \sqrt{(p^2 - q^2)^2 + (2\vec{p} \cdot \vec{q})^2}} \tag{3.8}$$

The parameter α represents the phase of the ellipse, i.e. α denotes the time trough ω which the oscillation needs to align with the long axes of the ellipse, as can be seen from figure 2.1. For further reference, α will also be referred to as the phase, this phase is defined with respect to the long axes of the ellipse. At time 0, the electric field vector is in the point (V_x,V_y), which is $\vec{p}$, α/ω time later, the electric field vector is aligned with the long axes of the ellipse, see equation 3.6. The angle ϕ denotes the angle between $\vec{p}$ and the long axes, it relates to α trough $\tan\phi = b/a \tan\alpha$. Remember that the polarisation ellipse is no longer defined in one plane. The parameters ϵ and α are defined in the rotation frame of the ellipse, independent of the external axes you choose.

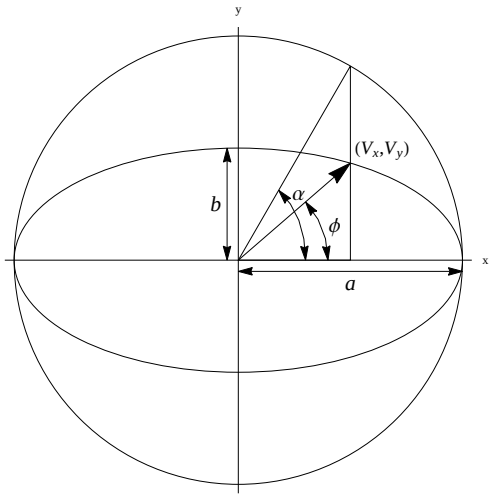

Figure 3.1: schematic representation of the phase α.

Each ellipse also has a handedness, i.e. whether the electric vector rotates clockwise or counterclockwise with respect to a reference frame. We can distinguish these cases by the sign of the scalar triple product $[\vec{p}, \vec{q}, \nabla\alpha] \equiv \vec{p} \cdot (\vec{p} \times \nabla\alpha)$.

3.3 Determining polarization singularities

By definition, one of the properties of polarization singularities, is that they are a singularity and occupy zero space. This means that one would only expect to find them in one mathematical point in space, this makes it nearly impossible to find the exact singularity. Typically they are found by investigating traces of a singularity in their expected neighbourhood, and our further efforts will be directed towards that goal.
At a C-point, the polarisation is perfectly circular and α is undetermined, because there is no long axes to align with. There is a subtle difference in the 3D situation compared to using the same procedure in 2D. The oscillation plane can now be different for every point space, therefore it is no longer possible to define an orientation angle, which is the angle between the long axes and the x axes of your reference plane. Instead, we can use the property that α/ω denotes the time needed to align with the long axes. The original argument can still be used: if the time needed to reach the long axes can not be determined, the electric field vector describes a circle, since then there is no long axes defined to align with.
We can exploit this fact by calculating so-called isogyres of α in the neighbourhood of local field fluctuations, if the contours converge unto one point, α cannot be determined and is therefore perfectly circular polarised. We can also expect ellipticity to increase around a singularity.
A singularity also caries angular momentum, comparable to the polarisation of photons. This momentum can be either positive or negative, depending on the handedness. However, there is still conservation of momentum throughout the system, to meet this requirement, polarisation singularities always appear in pairs. One has a negative value and the other has the same positive value.
For further inquiry into the value of angular momentum one can use Laurent series and Cauchy integrals, which allow for the calculation of the 'charge' of the singularity.

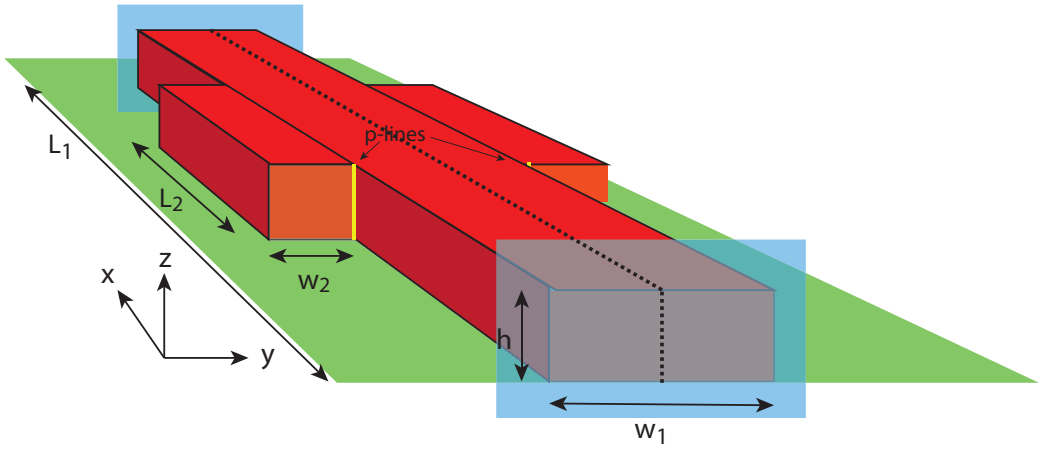

Figure 3.2: Schematic overview of the 3D model with periodic extrusions. The light blue planes indicate the periodic boundary planes, the green plane indicates the glass substrate. The dashed line denotes the symmetry plane. P-lines indicate areas of interest for the convergence behaviour as we will see later.

3.4 Field convergence behaviour for different mesh

The calculation of polarisation singularities depends on the electric field vector. Convergence of the eigenfrequency is reached with a relatively coarse mesh design with a smallest element size of 20nm. The Electric field profiles however are much more sensitive to changes in mesh design and can still vary at a smallest mesh size of 20nm. For calculation of polarisation singularities it is necessary that the Electric field is converged. In this section we discuss the effect of mesh size on the convergence of the electric fields.

3.4.1 Structural geometry

The structure we investigate is a single straight wire with periodic cuboid extrusions on the side, as depicted in figure 3.2. This structure lies on a glass substrate with a refractive index of 1.5 and has air above. The mesh is chosen such that in an area of at least 15nm around the structure the element size is determined, away from that area the maximum element size can grow with a factor 1.5 compared to it's neighbouring elements. The origin of this system is chosen for x in the middle of the drawn structure, in the middle of the bulges, for y in the middle of the wire at the dashed line and for z at the glass interface.

3.4.2 Mesh convergence

In order to test whether the electric field converges for this structural geometry and associated mesh, a line cut is taken along the edge of the wire. This is done for a geometry with L_1 is 500nm, L_2 is 350nm, h is 60nm, w_1 is 60nm and w_2 is 30nm referring to figure 3.2. The cut line is then directed in the x-direction and located at a height of 60nm and a width of 30nm. Although the found eigenmode may depend on the values of the spacial parameters of the model and the chosen k_x, the convergence of this mesh design will be unaffected by such changes.
The maximum element size in the area around the wire is now varied. Since the amplitude of the eigenmode is arbitrary, the curves are normalised such that the area under each curve equals one. As can be seen from figure 3.3 starting from a maximum element size of 12nm the field profile converges in most areas. However, near the transition from edge of the nanowire to surface of the nanowire, illustrated with the p-lines (four per period), there is a peak in the amplitude, which does not converge for these maximum mesh sizes. 7nm is the highest possible value for this mesh configuration due to RAM limitation. Something interesting is going on around the p-lines.

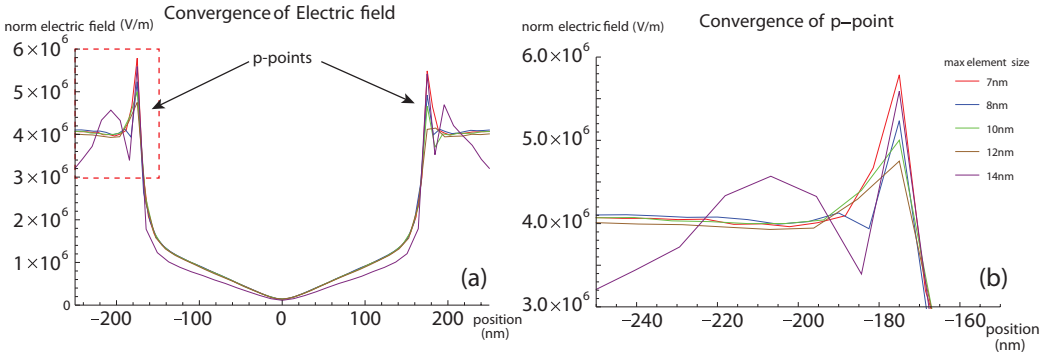

Figure 3.3: Convergence plot for different maximum element sizes. (a) the norm of the electric field along the entire length of the wire. (b) zoom in on the red dashed box from (a) for convergence around a p-point. The Floquet k-vector used is $k_x = \pi \ / \ L_1 = 6.28 \times 10^6 \ m^{-1}$ and has a resulting frequency of $\nu = 1.86 \times 10^{14}$Hz.

3.5 Mode profiles

We have seen that there are local field fluctuations around the p-lines and that these do not converge yet for a mesh size of 7nm. In order to investigate the p-lines further, we altered the mesh such that the maximum element size around one p-line is 1.5nm, the area of this extra precision is denoted with the black box around the (c) indicated dashed line in (a) of figure 3.4. To compensate for this extra usage of memory, the maximum element size in the rest of the geometry is made courser up to 15nm element size around the wire. If we investigate the mode profile, we see that the electric field is still concentrated around the surface of the wire, however the field intensity is no longer homogeneously in the x-direction. We see that there exists an enhanced field around the extrusion zone, predominantly so at the outer corners of the extrusion. As we already saw in figure 3.3, the intensity of the electric field at the corners of the structure increase with a finer mesh. The same effect can be seen in figure 3.4(a), where the intensity on the left corner is higher than the intensity on the right corner. If we look carefully at 3.4(c) we see that there exists electric field around the p-line.

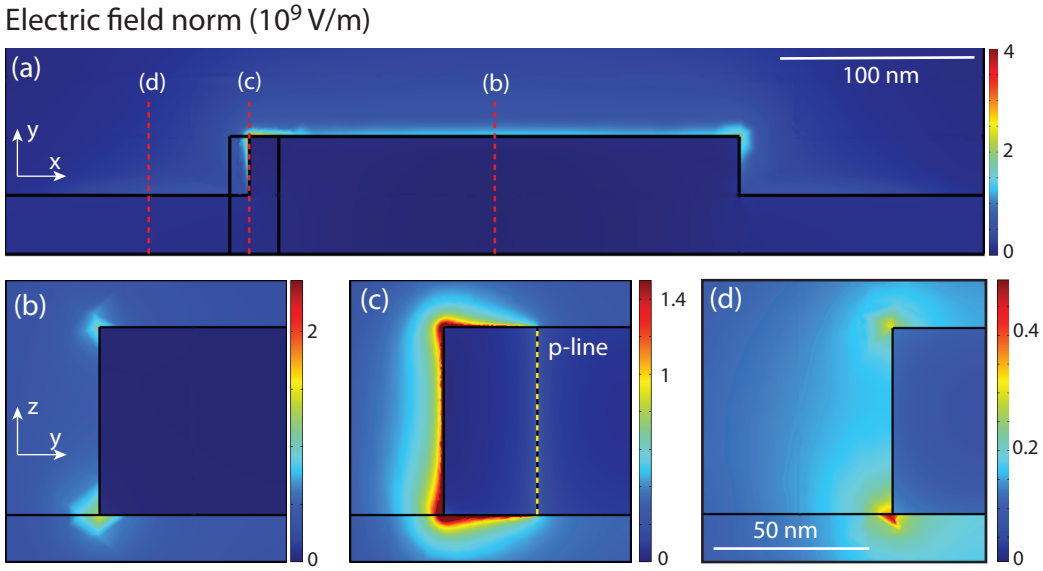

Figure 3.4: Electric mode profile of periodic structure. The eigenmode has a frequency of 178THz for $k_x = 6.28\ 10^6$. (a) is a view from the scanning plane at $z = 0$nm. (b-d) are cross cuts in yz taken at $x = 0, -125$ and -200nm respectively. Inset in (a) are the positions of these cross cuts on the wire.

The magnetic field of the mode is localised away from the extrusion (see

fig 3.5), whereas the electric field is localised mostly at the extrusion. We see significant fields inside the wire. Using the magnetic field, we see a charge movement inside the wire. With the use of Ampère's Law, we notice that the electric current vector is orientated away from the extrusion, i.e. charge flows away from the extrusion. If we consider that this image is a snapshot taken in time of an oscillating wave, we expect the charge to move in the opposite direction after a half period. The magnetic field is mostly oriented in the yz plane, perpendicular to the propagating direction, but has a significant x-component around the p-lines and at the outer corners (not shown).

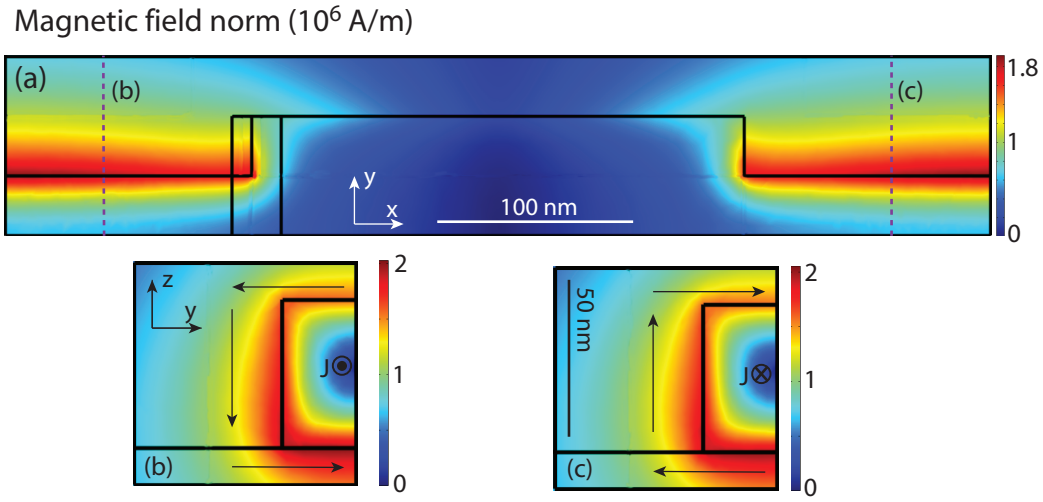

Figure 3.5: Magnetic mode profile for the same eigenmode as in 3.4. (a) is a view from the scanning plane at $z = 20$nm. (b,c) are cross cuts in yz taken at $-200nm$ and $200nm$ respectively, as indicated with the purple dashed lines in (a). The arrows schematically indicate the direction of the field, as viewed coming from the left in (a). The resulting $\vec{J}$ is drawn.

3.6 Singularities at p-lines

In this section we will use the mathematics developed in 3.2 to investigate the occurrence of polarisation singularities near the p lines. The electric field in the coarser mesh shows differences compared to previous finer mesh, however this does not influence the ability to find the eigenmode, only the structure and intensity of the *local* field. As can be seen in figure 3.6, polarisation singularities seem to appear at the surface of the metal. As a first case, we changed the model such that the nanowire is embedded in glass. This

creates an extra symmetry plane. We measure two peaks in the ellipticity and we notice that the contours of α intersect at these peaks. These peaks are symmetric as a result from the extra symmetry. Using the triple product $[\vec{p}, \vec{q}, \nabla\alpha]$, we see that the ellipticity around these peaks indeed has opposite handedness. There is no intersection of alpha contours at the "wave" of ellipticity at -45nm, this is no polarisation singularity, but rather there appears to be some energy flow. Please note that the k_x used is exactly at the edge of the Brillioun zone, which generates modes at the stop gap.

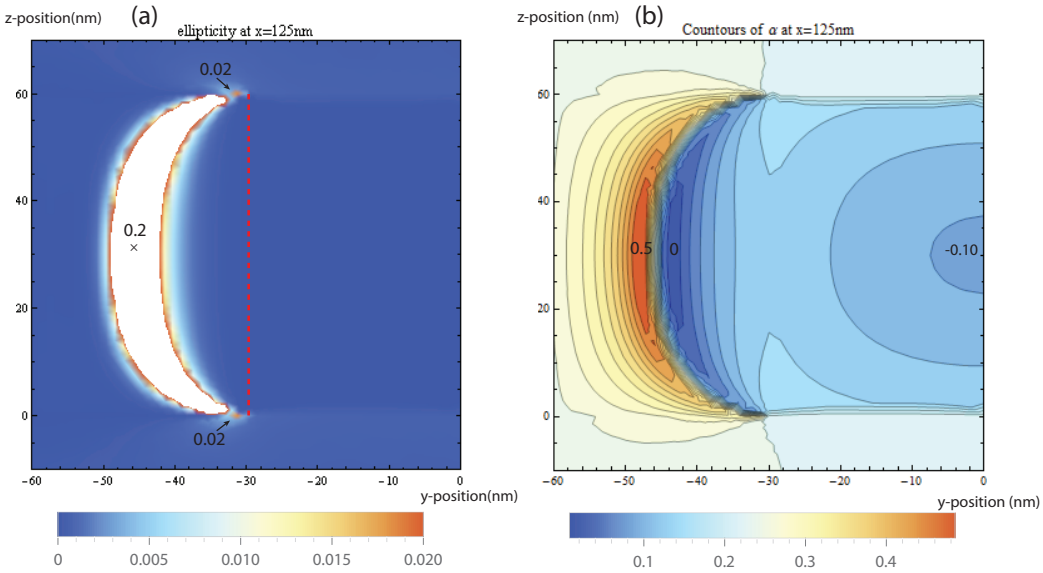

Figure 3.6: Nanowire embedded in glass, a yz cut is taken at $x = 125nm$, at the edge of the extrusion. Extrema are noted with their numeric values. The eigenmode found has a frequency of 186THz and a Floquet k-vector k_x of 6.28 10^6.(a) is a plot of the ellipticity, two peaks are visible at $y = -30nm$ and z={0,60}. There is a "wave" of ellipticity near $y = -45nm$. The red dashed line indicates the p-line. To the left between $y = -30nm$ and $y = -60nm$ is the interface between gold and glass at the edge of the extrusion. (b) contourplot of the phase, the contours intersect at the peaks visible in (a).

Next we look at the more complicated case of a glass substrate with air above, the most pronounced singularities appear at $x = 126nm$. As can be seen in figure 3.7, we measure two sharp peaks in the ellipticity and we notice again that the contours of α intersect at these peaks. The peak near the glass interface at z is $0nm$ is the most pronounced due to the higher refractive index of glass. Again we see that the ellipticity around these peaks

has opposite handedness.

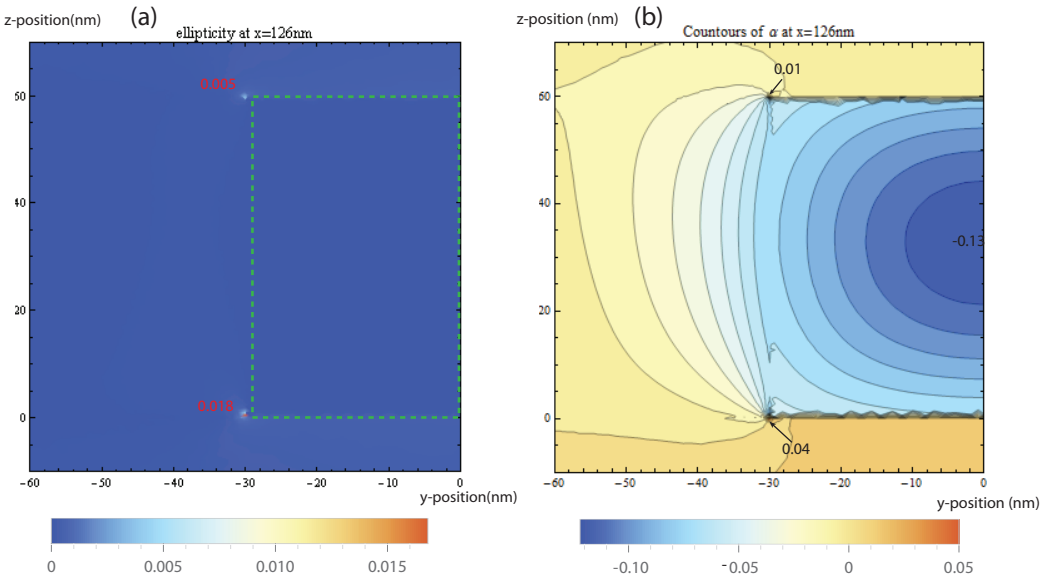

Figure 3.7: A yz-cut is taken at x=126nm for the situation illustrated in figure 3.2 with a glass substrate and air above, just out of the extrusion and zoomed on the area of the nanowire. The eigenmode has a frequency of 178THz for $k_x = 6.28\ 10^6$. (a) shows the ellipticity, there are two peaks visible with inset amplitudes at y=-30nm, z=0nm and z=60nm for the peaks near the glass and at the top respectively. The green dashed square indicates the gold boundary.(b) is a contourplot of the phase, the contours appear to intersect at the same place as in (a).

3.7 Conclusions and outlook

We conclude that indeed polarisation singularities can exist on plasmonic nanowires with periodic extrusions. We have calculated them to be at the surface of the metal near so-named p-lines. Although the amplitude of the ellipticity does not reach very near to 1, i.e. a perfect circle, we do see that these peaks stand out clearly and that the contours of alpha cross exactly at these peaks. Furthermore we have seen that they appear in pairs and that they have opposite handedness. We also see that the mode profile shows different behaviour from straight nanowires. By doing these calculations, we have demonstrated that current computational power is sufficient to find these singularities and that there is no immediate need to resort to super-computing.

In order to effectively couple quantum dots to the polarisation singularities, it is necessary to place the quantum dots at the singularity. This is only possible if the singularity is some distance away from the metal and this has not been found. However, now that a model exists to calculate singularities in 3D, it is possible to sweep the parameters of the structure, exploring new geometries of the structure and, most notably, sweep the Floquet k-vector along the Brillioun zone to find polarisation singularities away from the surface of the metal. Future work should also include finding quantitative agreement on known properties between 3D and 2D models.

Bibliography

[1] Matteo Burresi, RJP Engelen, Aron Opheij, Dries van Oosten, D Mori, T Baba, and L Kuipers. Observation of polarization singularities at the nanoscale. *Physical review letters*, 102(3):033902, 2009.

[2] Heinz Raether. Surface plasmons on smooth and rough surfaces and on gratings. *Springer tracts in modern physics*, 111, 1988.

[3] P. Drude. Zur Elektronentheorie der Metalle. *Annalen der Physik*, 306:566–613, 1900.

[4] Ewold Verhagen, Marko Spasenović, Albert Polman, and L Kuipers. Nanowire plasmon excitation by adiabatic mode transformation. *Physical review letters*, 102(20):203904, 2009.

[5] Ewold Verhagen. *Subwavelength light confinement with surface plasmon polaritons*. PhD thesis, Utrecht University, 2009.

[6] William L Barnes, Alain Dereux, and Thomas W Ebbesen. Surface plasmon subwavelength optics. *Nature*, 424(6950):824–830, 2003.

[7] Stephen D. Gedney. *Periodic structures and Floquet's Theorem*. University of Kentucky, Electrical Engeneering, 2007. reader for computational electrodynamics.

[8] William H Press, Saul A Teukolsky, William T Vetterling, and Brian P Flannery. *Numerical recipes 3rd edition: The art of scientific computing*. Cambridge university press, 2007.

[9] Masanori Koshiba, Kazuya Hayata, and Michio Suzuki. Improved finite-element formulation in terms of the magnetic field vector for dielectric waveguides. *Microwave Theory and Techniques, IEEE Transactions on*, 33(3):227–233, 1985.

[10] Alexandre Archambault, Tatiana V Teperik, François Marquier, and Jean-Jacques Greffet. Surface plasmon fourier optics. *Physical Review B*, 79(19):195414, 2009.

[11] Emil Wolf and Max Born. *Principles of optics*. Pergamon press, 1965.

Acknowledgements

It has been a privilege to do my bachelors thesis at AMOLF, to be able to experience research in such a notable institute with so many inspired and enthusiastic people around. There are many people whom I want to thank and without whom I would not have been able to make this thesis. First and foremost I'd like to thank my supervisors Kobus Kuipers and Anouk de Hoogh. I want to thank Kobus for the guidance and allowing me to do my thesis in his group, he managed to inspire me such, that after one talk I was sold and decided I wanted to do my thesis at AMOLF. I want to thank Anouk for being my direct supervisor with so much patience, enthusiasm and good cares. She really took the time to show me around. I'd also like to thank Boris le Feber and Matthias Wulf for all the useful discussions and explanations we've had, Nir Rotenberg for taking the time to criticize my manuscript and all the other members of our Nano Optics group for all the input and the good atmosphere.
AMOLF has a very good infrastructure and I'd especially like to thank the people from ict Wiebe de Boer and Jan van Elst, who made my life a lot easier. In general I'd like to thank all the people at AMOLF and the center for nanophotonics for all the conversations we've had during the nanophotonics colloquium and coffee breaks, specifically my roommate Andrej Kwadrin for all the good times and discussions. A special thanks goes to Ewold Verhagen, whose work made my own research possible. He was always willing to make time and help me understand the problems I faced with great enthusiasm.